Article:

Smith, C.C. and Cubrinovski, M. (2011) Pseudo-static limit analysis by discontinuity layout optimization: Application to seismic analysis of retaining walls. Soil Dynamics and Earthquake Engineering, 31 (10). pp. 1311-1323. ISSN: 0267-7261

https://doi.org/10.1016/j.soildyn.2011.03.014

Pseudo-static limit analysis by discontinuity layout optimization: application to seismic analysis of retaining walls

C.C. Smith[a], M. Cubrinovski[b]

[a]*Department of Civil and Structural Engineering, University of Sheffield, Sheffield, UK*
[b]*Department of Civil and Natural Resources Engineering, University of Canterbury, Christchurch, New Zealand*

Abstract

Discontinuity Layout Optimization (DLO) is a recent development in the field of computational limit analysis, and to date, the literature has examined the solution of static geotechnical stability problems only by this method. In this paper the DLO method is extended to the solution of seismic problems though the use of the pseudo-static approach. The method is first validated against the solutions of Mononobe-Okabe and Richards and Elms for the seismic stability of retaining walls, and then used to study the effect of a wider range of failure modes. This is shown to significantly affect the predicted stability. A framework for modelling water pressures in the analysis is then proposed. Finally an example application of the method is illustrated through the assessment of two quay walls subjected to the Kobe earthquake.

Key words: retaining wall, Discontinuity Layout Optimization, limit analysis, limit equilibrium, pseudo-static method, seismic stability

1. Introduction

Various methods have been developed for seismic analysis of retaining structures ranging from simplified pseudo-static methods to sophisticated dynamic numerical procedures in which detailed response of the soil-structure system is considered including effects of excess pore water pressures and complex stress-strain behaviour of soils [1]. Key objectives in the assessment of seismic performance of retaining walls are to estimate the threshold acceleration (earthquake load) required for triggering instability of the system and to estimate the permanent wall displacements caused by earthquakes.

In the simplified approach, these objectives are achieved in two separate calculation steps. In the first step, a pseudo-static analysis typically based on the conventional limit equilibrium approach is conducted to estimate the threshold acceleration level required for onset of permanent wall displacements. In this analysis, the seismic earth pressure from the backfill soils is commonly approximated by the Mononobe-Okabe solution ([2]; [3]). In the second calculation step, a simplified dynamic analysis is carried out in which the displacement of the wall due to an earthquake is estimated using a rigid sliding block analogy ([4]; [5]). Strictly speaking, the Mononobe-Okabe method is applicable only to gravity retaining walls that undergo relatively large displacements and develop the active state of earth pressures in the backfills. Even for these cases the method is seen only as a relatively crude approximation of the complex seismic interaction of the soil-wall system and ground failure in the backfills. Experimental evidence suggests however that the dynamic earth pressure estimated by the Mononobe-Okabe solution is reasonably accurate provided that the method is applied to a relevant problem ([6]; [7]) and with an appropriate value for the effective angle of shearing resistance ϕ'.

In this context, a modification of the Mononobe-Okabe method and alternative simplified pseudo-static approaches have been recently proposed allowing for a progressive failure in the backfills ([8]; [9]). The single most significant shortcoming of the simplified pseudo-static approach arises from the assumption that dynamic loads can be idealized as static actions. In the case of gravity retaining walls, the key questions resulting from this approximation are what is the appropriate level (acceleration or seismic coefficient) for the equivalent static load and how to combine effects of seismic earth pressures and inertial loads in the equivalent static analysis. Clear rules for the definition of the equivalent static actions have not been established yet, thus highlighting the need for systematic parametric studies when using the pseudo-static approach for assessment of the seismic performance of retaining structures.

In spite of these limitations however, classical theories and simplified solutions based on these theories are likely to remain of practical value even when sophisticated deformation analyses are readily available. This is particularly true for problems involving significant uncertainties in soil parameters, field conditions, stress-strain behaviour of soils and earthquake loads (e.g., representative ground motion at a given site). One may argue that the simplified and advanced methods of analysis have different roles in the seismic assessment, and that they address different aspects of the problem and are essentially complementary in nature ([10]). The need for further development of both simplified pseudo-static methods and advanced numerical procedures for seismic analysis has been also recognized within the emerging Performance Based Earthquake Engineering (PBEE) framework and its implementation in the geotechnical practice ([11]).

This paper presents an alternative approach for pseudo static analysis of retaining walls based on the recently developed limit analysis method: discontinuity layout optimization (DLO). The proposed approach retains the qualities of the simplified analysis while offering an increased versatility in the modelling and more realistic idealization of the failure mechanism as compared to that of the Mononobe-Okabe method. The key aims of this paper are to:

1. Extend the DLO procedure to include the solution of problems involving earthquake loading using the pseudo-static method
2. Verify the DLO results against the results of Mononobe-Okabe and Richard and Elms [5] by undertaking a parametric study of the influence of soil angle of shearing resistance ϕ', soil-wall interface angle of shearing resistance δ', slope angle β, inclination of wall back to vertical θ, cohesion intercept c', wall inertia, and water pressures. These studies will be undertaken by using a DLO solution constrained to generate solutions of the simple form adopted by these workers.
3. Examine the influence on stability when considering combined sliding, bearing and overturning failure mechanisms, using an unrestricted DLO analysis.
4. Outline the principles for incorporating the modelling of water pressures in the DLO analysis following the work of Matsuzawa et al. [12].
5. Illustrate the application of the method to two case studies.

2. Discontinuity Layout Optimization

Discontinuity Layout Optimisation (DLO) is a recently developed numerical limit analysis procedure [13] which can be applied to a broad range of engineering stability problems. In the current paper it is demonstrated that the basic DLO method can be extended to the solution of seismic geotechnical stability problems though the use of the pseudo-static approach.

Instead of using an approach which requires discretisation of the problem into solid elements (as with e.g. finite element limit analysis), DLO plane plasticity problems are formulated entirely in terms of lines of discontinuity, with the ultimate objective being to identify the arrangement of discontinuities present in the failure mechanism corresponding to the minimum upper bound load factor. Although formulated in terms of lines of discontinuity, or slip-lines, the end result is that DLO effectively automates the traditional 'upper bound' hand limit analysis procedure (which involves discretising the problem domain into various arrangements of sliding rigid blocks until the mechanism with the lowest internal energy dissipation is found).

In order to obtain an accurate solution a large number of potentially active discontinuities must be considered. To achieve this, closely spaced nodes are distributed across the problem domain, and potentially active discontinuities inter-connecting each node to every other node are added to the problem. A simple example of the active failure of a rough retaining wall is given in Fig. 1. The fine lines indicate the set of potential discontinuities (for clarity only the shorter ones have been shown). The DLO procedure is formulated as a linear programming (LP) problem that identifies the optimal subset of discontinuities that produces a compatible mechanism with the lowest energy dissipation (highlighted lines).

The accuracy of the result is dependent on the prescribed nodal spacing. In this example there are $n = 30$ nodes and thus $m = n(n-1)/2 = 435$ potential discontinuities (including overlapping discontinuities of differing lengths). It can be shown that there are of the order of $2^m = 2^{435}$ possible different arrangements of these discontinuities. From this set the DLO procedure identifies the optimal compatible mechanism. At first sight the magnitude of the problem size seems intractable, but with careful formulation it can be solved.

A particular advantage of the procedure is the ease with which singularities in the problem can be handled, with no *a priori* knowledge of the likely form of the solution being required. It should be noted that, in contrast with upper and lower bound finite element limit analysis, with DLO no attempt is made to model deformations within 'elements' / sliding blocks. Instead the large number of potential discontinuities considered ensure that the essential mode of the deformation is captured.

A detailed description of the development of the numerical formulation of DLO may be found in [13]. The core matrix formulation is reproduced below. The primal kinematic problem formulation for the plane strain analysis of a quasi-statically loaded, perfectly plastic cohesive-frictional body discretized

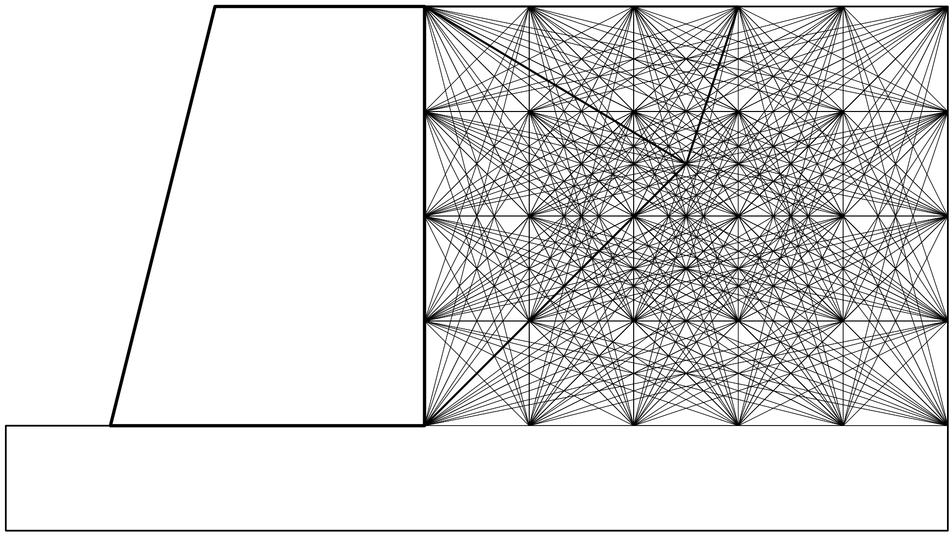

Figure 1: Example DLO solution to the problem of the active pressure on a rough retaining wall. Fine lines are set of potential discontinuities (input data). Thick lines represent those discontinuities that form the critical collapse mechanism based on the set of starting discontinuities (computed solution)

using m nodal connections (slip-line discontinuities), n nodes and a single load case can be stated as follows:

$$\min \lambda \mathbf{f}_{\mathrm{L}}^{T}\mathbf{d} = -\mathbf{f}_{\mathrm{D}}^{T}\mathbf{d} + \mathbf{g}^{T}\mathbf{p} \tag{1}$$

subject to:

$$\mathbf{Bd} = \mathbf{0} \tag{2}$$

$$\mathbf{Np} - \mathbf{d} = \mathbf{0} \tag{3}$$

$$\mathbf{f}_{\mathrm{L}}^{T}\mathbf{d} = 1 \tag{4}$$

$$\mathbf{p} \geq \mathbf{0} \tag{5}$$

where $\mathbf{f}_{\mathrm{D}}$ and $\mathbf{f}_{\mathrm{L}}$ are vectors containing respectively specified dead and live loads, $\mathbf{d}$ contains displacements along the discontinuities, where $\mathbf{d}^{T} = \{s_1, n_1, s_2, n_2 ... n_m\}$, where s_i and n_i are the relative shear and normal displacements between blocks at discontinuity i; $\mathbf{g}^{T} = \{c_1 l_1, c_1 l_1, c_2 l_2, ... c_m l_m\}$, where l_i and c_i are respectively the length and cohesive shear strength of discontinuity i. $\mathbf{B}$ is a suitable $(2n \times 2m)$ compatibility matrix, $\mathbf{N}$ is a suitable $(2m \times 2m)$ flow matrix and $\mathbf{p}$ is a $(2m)$ vector of plastic multipliers. The discontinuity displacements in $\mathbf{d}$ and the plastic multipliers in $\mathbf{p}$ are the LP variables.

In the derivation of the pseudo-static approach, only the representation of the dead and live loads are of specific interest here. (Further details of the development of DLO and its application to static plasticity problems are described in [13]).

3. Extension of DLO theory to pseudo-static analysis

In a pseudo static analysis, the imposition of horizontal and vertical seismic acceleration within the system results in additional work terms in the governing equation that are analogous to that for self weight (*i.e.* body forces). The work term for vertical movement will first be examined. Here the contribution made by discontinuity i to the $\mathbf{f}_{\mathrm{D}}^T\mathbf{d}$ term in Eq. (1) can be written as follows [13] and is formulated to include a vertical pseudo-static acceleration coefficient k_v (assumed to act upward) :

$$\mathbf{f}_{\mathrm{D}i}^T\mathbf{d}_i = (1-k_v)\begin{bmatrix} -W_i\beta_i & -W_i\alpha_i \end{bmatrix}\begin{bmatrix} s_i \\ n_i \end{bmatrix} \tag{6}$$

where W_i is the total weight of the strip of material lying vertically above discontinuity i, and α_i and β_i are the horizontal and vertical direction cosines of the discontinuity in question. The equation simply calculates the work done against gravity and pseudo static acceleration by the vertical component of motion of the mass of the strip of soil vertically above the discontinuity. Choice of the vertical for the strip of soil is arbitrary. The direction does not matter as long as it is consistent throughout the problem. The fact that there may be multiple whole and partial other slip-lines causing additional deformation above this slip-line does not affect the calculation since all deformation is measured in relative terms. The work equations are simply additive in effect as each slip-line is considered. In the equations, the adopted sign convention is that s is taken as positive clockwise; for an observer located on one side of a discontinuity, the material on the other side would appear to be moving in a clockwise direction relative to the observer for positive s.

To include work in the horizontal direction assuming a horizontal pseudo-static acceleration coefficient k_h (taken as positive in the -ve x-direction), this equation must be modified as follows:

$$\mathbf{f}_{\mathrm{D}i}^T\mathbf{d}_i = \left\{(1-k_v)\left[\begin{array}{cc} -W_i\beta_i & -W_i\alpha_i \end{array}\right] + k_h\left[\begin{array}{cc} -W_i\alpha_i & W_i\beta_i \end{array}\right]\right\}\left[\begin{array}{c} s_i \\ n_i \end{array}\right] \quad (7)$$

The right hand term in the curly brackets represents the work done by the horizontal movement of the body of soil lying vertically above the slip-line.

The DLO method finds the optimal collapse mechanism for the problem studied. In order to achieve this it must increase loading somewhere within the system until collapse is achieved, by applying what is termed the 'adequacy factor' to a given load. In the case of seismic loading it is convenient to apply this factor to the horizontal acceleration itself (or simultaneously to the horizontal and vertical acceleration). In effect the question posed to the method is 'how large does the horizontal acceleration have to be for the triggering of instability or the onset of permanent displacements to occur'. Note that this is somewhat different from conventional approaches using *e.g.* the Mononobe-Okabe solutions where a horizontal acceleration is prescribed and a corresponding active thrust computed, but is considered a more realistic and convenient form for practical engineering design and analysis.

To apply live loading to both the horizontal and vertical accelerations, the $\mathbf{f}_{\mathrm{D}}^T\mathbf{d}$ term in Eq. (1) is not modified, instead the equation is modified such that the $\mathbf{f}_{\mathrm{L}}^T\mathbf{d}$ term becomes as follows (for slip-line i):

$$\mathbf{f}_{\mathrm{L}i}^T\mathbf{d}_i = \left\{k_v\left[\begin{array}{cc} -W_i\beta_i & -W_i\alpha_i \end{array}\right] + k_h\left[\begin{array}{cc} -W_i\alpha_i & W_i\beta_i \end{array}\right]\right\}\left[\begin{array}{c} s_i \\ n_i \end{array}\right] \quad (8)$$

In the following sections, the DLO approach (as implemented in the software LimitState:GEO [14]) will be compared to a number of analyses from the literature. As with any numerical method, the results can be sensitive to the nodal distribution employed. Some details of the analysis configuration are therefore listed in Appendix A to facilitate the reproduction of any analysis.

4. Verification of DLO against the Mononobe-Okabe solutions

4.1. Dry conditions

A number of parametric studies were undertaken, examining the variation of active thrust (P_{AE}) against the horizontal acceleration coefficient (k_h) for various values of soil/wall interface friction δ', slope angle β, and soil angle of shearing resistance ϕ'. In order to compare with the Mononobe-Okabe method [2], [3], it is necessary to apply a fixed resistance to the active force and allow the DLO method to find k_h. The dependent and independent variables are thus the reverse for the Mononobe-Okabe method, but the results will be plotted as is conventional for the latter approach. The core equations for determining the horizontal thrust by the Mononobe-Okabe method are presented in Appendix B and will be further developed in later sections. The notation used in these equations and the rest of the paper is listed in Appendix C.

The DLO model used for this study is shown in Fig. 2. Here the wall is modelled as a weightless rigid material resting on a smooth rigid surface. The wall has unit height and the soil has unit weight. The prescribed active force is applied to the left hand vertical face of the block. The soil/wall interface is modelled with interface angle of shearing resistance δ'. In this model the wall slides horizontally only. No nodes were applied to the soil body itself, rather they were permitted only on the surface and at the vertices (*e.g.* wall corners). This was done in order to force a single wedge failure mechanism required for direct comparison with the Mononobe-Okabe solutions, as depicted in Fig. 2.

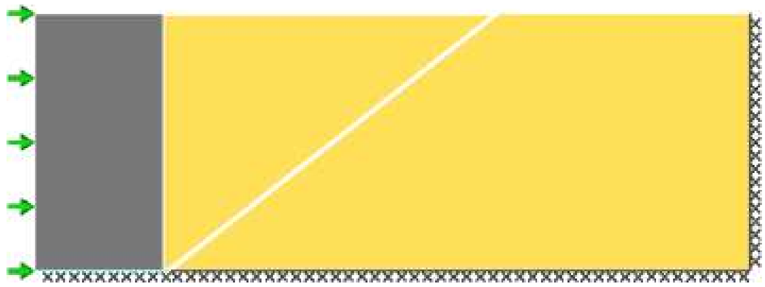

Figure 2: Single wedge failure mechanism for $k_h = 0.25$, $\delta = \phi = 30^o$ (active force $0.231\gamma H^2$). Wedge angle is much shallower than static case as expected.

Comparisons between seismic earth pressures computed using the DLO approach and Mononobe-Okabe theory are shown in Figures 3, 4 and 5 for various values of ϕ', δ' and β in terms of soil unit weight γ and wall height H.

The results demonstrate that the DLO results match exactly with the Mononobe Okabe theory except for small deviations at higher accelerations.

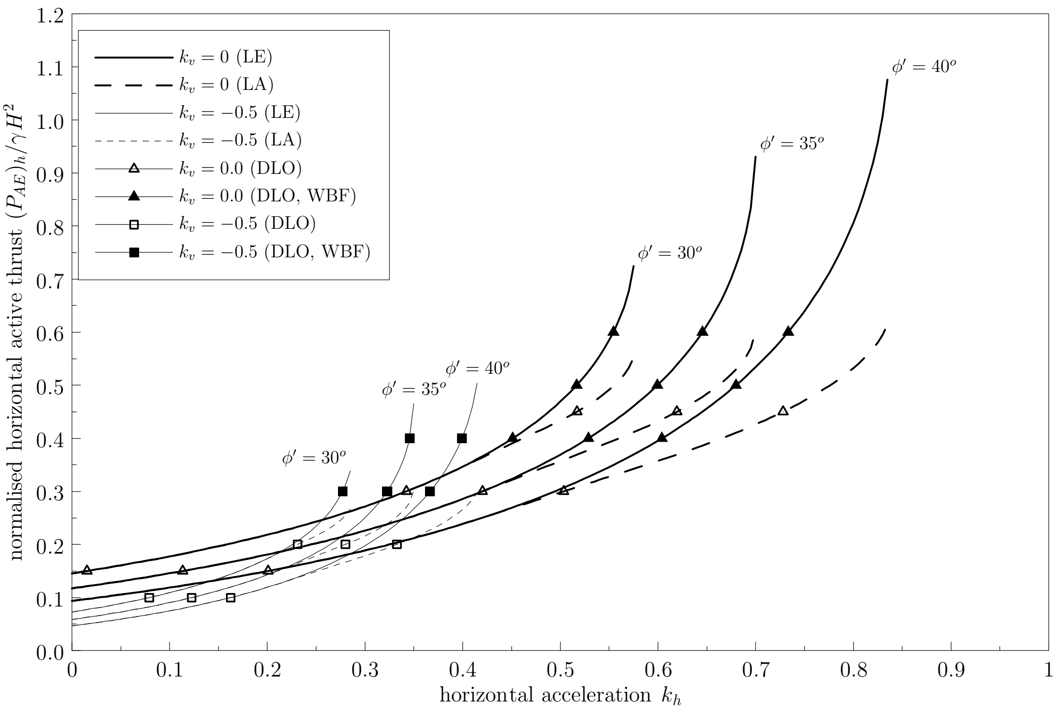

Figure 3: Plot of $P_{AE}\cos\delta'/\gamma H^2$ vs. k_h, for various ϕ' (30^o, 35^o, 40^o), $k_v = 0.0, -0.5$, $\beta = 0^o$, $\delta' = 0.5\phi'$. Limit Equilibrium (LE) and Limit Analysis (LA) theoretical results are plotted as lines, and DLO results as markers. (WBF=wall base modelled as frictional).

These arise from the fact that Mononobe-Okabe is a limit equilibrium approach, while DLO is a limit analysis approach. The former method does not include an explicit consideration of the problem kinematics, while the latter employs an associative flow rule, whereby any shearing is assumed to be accompanied by dilation equal to the angle of shearing resistance. In certain circumstances, the direction of relative movement between soil and wall can reverse for a limit analysis, thus reversing the direction of the wall/soil interface shear force. A limit analysis description of the Mononobe-Okabe solution for horizontal wall movement is presented in Appendix D, and the results from this formulation plotted as dashed lines in Figures 3, 4 and 5. It can be seen that the DLO results match the dashed lines exactly.

Additionally, DLO analysis was undertaken modelling the wall base ground interface as frictional (equal to ϕ'). As the wall slides, dilation gives it a ver-

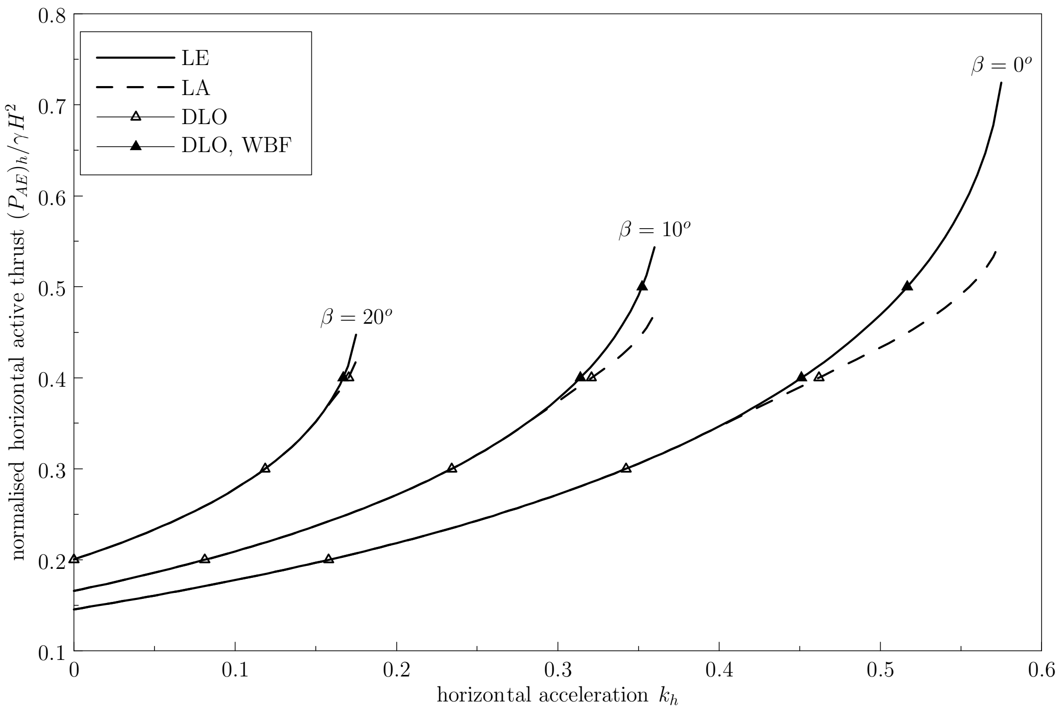

Figure 4: Plot of $P_{AE} \cos\delta'/\gamma H^2$ vs. k_h, for various β (0^o, 10^o, 20^o), $k_v = 0.0$, $\phi = 30^o$, $\delta' = 0.5\phi'$. Theory and DLO results. Limit Equilibrium (LE) and Limit Analysis (LA) theoretical results are plotted as lines and DLO results as markers. (WBF=wall base modelled as frictional).

tical component of motion which will always be greater than the upward vertical movement of the soil wedge. This ensures that at all times the wall/soil shear force on the right hand side vertical face acts downwards on the wall as assumed in the Mononobe-Okabe solution. However the DLO result will now include an extra term relating to the base shear force. Equation 9 may be used to determine the equivalent Mononobe-Okabe active earth pressure, from the prescribed active force P_0 (assuming a weightless wall and translational movement only).

$$(P_0)_h = P_{AE} \cos(\delta' + \theta) \{1 - \tan(\delta' + \theta) \tan\phi'\} \tag{9}$$

The additional results are plotted using hollow symbols in Figures 3, 4 and 5. It can be seen that they exactly match the original Mononobe-Okabe

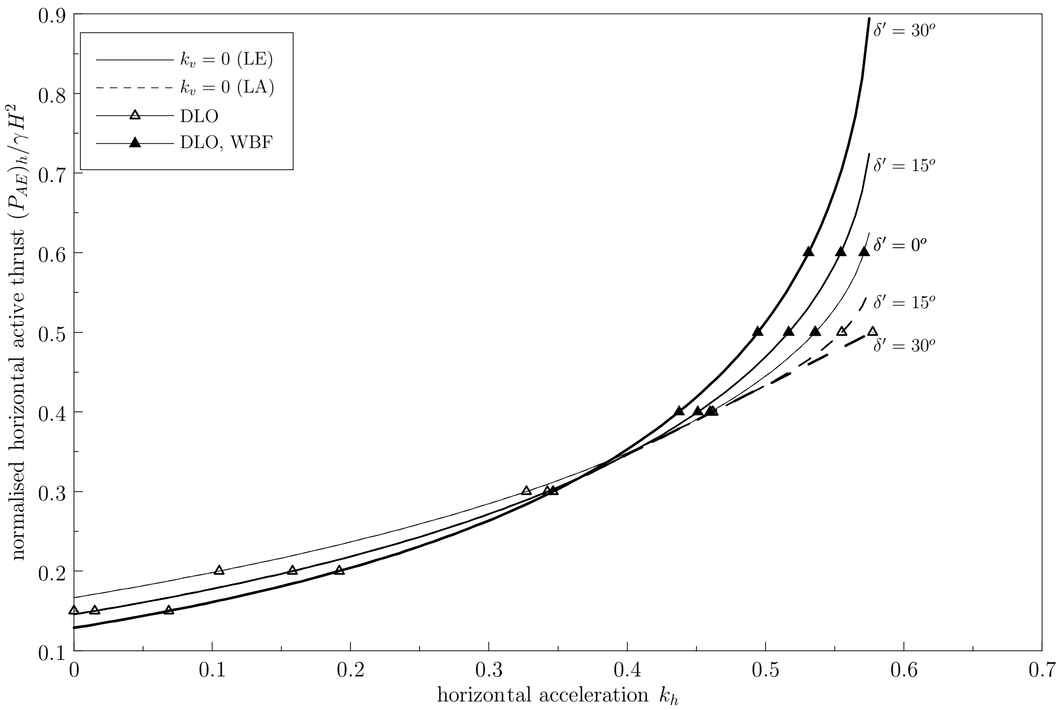

Figure 5: Plot of $P_{AE}\cos\delta'/\gamma H^2$ vs. k_h, for various δ' (0^o, 15^o, 30^o), $k_v = 0.0$, $\phi' = 30^o$, $\beta = 0^o$. Limit Equilibrium (LE) and Limit Analysis (LA) theoretical results are plotted as lines and DLO results as markers. (WBF=wall base modelled as frictional).

results.

4.2. Effect of cohesion

Prakash [15] provides equations for the determination of the seismic earth pressures on a wall retaining horizontal soil for a $c - \phi$ soil through modification of the Mononobe-Okabe equations. The equations are presented in Appendix E.

Comparisons between seismic earth pressures computed using equations from [15] and DLO are shown in Figure 6 for various values of ϕ', c' and show exact agreement.

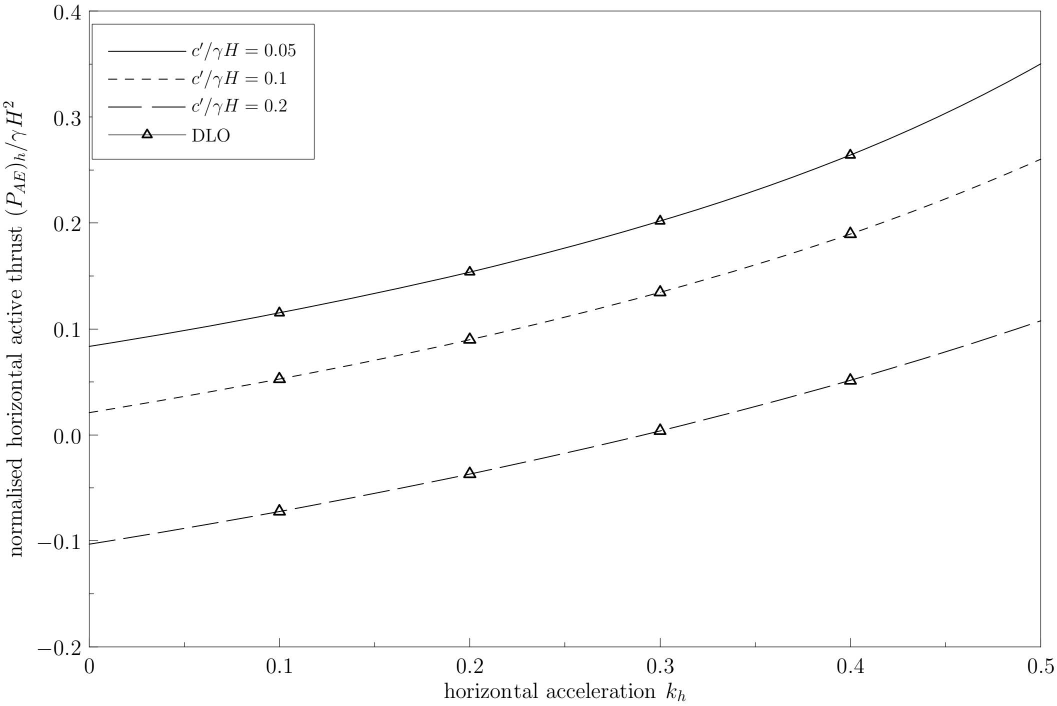

Figure 6: Plot of $P_{AE} \cos \delta' / \gamma H^2$ vs. k_h, for $\phi' = 30^o$, $c'/\gamma H = 0.05, 0.1, 0.2$, $\delta' = \phi'/2$, $c'_w = c'/2$. Theory (lines) and DLO results (symbols). DLO results are from an analysis constrained to generate a single wedge.

5. Extension to multiple wedge collapse mechanisms

In this series of analyses nodes were additionally placed within the soil body and on the wall back face in order to allow more complex mechanisms to be developed. For the static loading of rough walls, it is known that more complex slip-line patterns than that represented by a single wedge occur. Investigation of the problem indicated that the pseudo-static forces tend to reduce the effect of soil/wall interface friction, by rotating the resultant interface force and result generally in solutions very close to a single wedge type. Only at low accelerations do the mechanisms significantly change as depicted in Fig. 7. The change in corresponding results are marginal (<3%) even for the most critical problems with full friction wall/soil interfaces and horizontal soil surfaces as shown in Figure 8. Multiple slip-planes and curvature in the sliding surface near the base of the wall, as seen in Fig. 7, have been observed in numerical studies ([16]) and centrifuge tests ([17]) on retaining walls under earthquake loading.

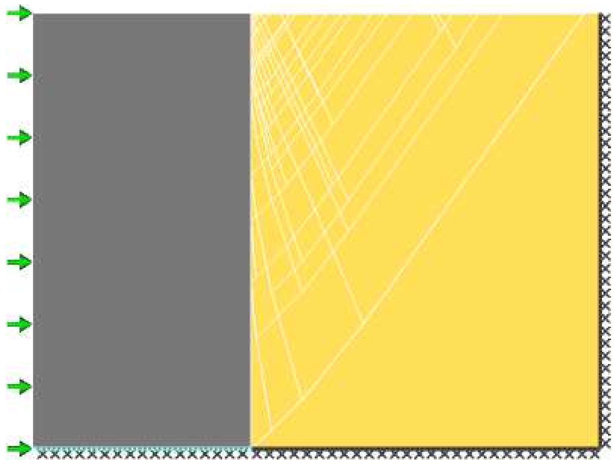

Figure 7: Failure mechanism for a fixed wall resistance of $0.15\gamma H^2$ and $\delta = \phi = 30^o$. Note the change in mechanism compared to Fig. 2. Collapse predicted in this case at $k_h = 0.060$ rather than $k_h = 0.069$ for the single wedge solution.

6. Influence of wall inertia

Richards and Elms [5] demonstrated that wall inertia has a significant effect on wall stability under earthquake loading. For this study the previous DLO model (shown in Fig. 7) was modified by including self weight for the wall and by modelling a wall base friction ϕ'_b. The wall has dimensions height H and width $0.5H$ and the mechanism was unconstrained. Strength parameters used by Richard and Elms were adopted for comparison purposes ($\phi' = \phi'_b = 35^o, \delta' = \phi'/2$).

Example results for a rigid base (pure sliding of the wall along the base) are shown with the solid line in Fig. 9 where the wall weight factor F_w (ratio of weight of wall required for dynamic stability divided by that required for static stability on a rigid base) is plotted against horizontal acceleration k_h. The results demonstrate that the DLO results match very closely with the theory of Richards and Elms (key equations from Richards and Elms are presented in Appendix F). This indicates that the single wedge analysis used in the closed form solution is a close representation of actual failure for these parameters.

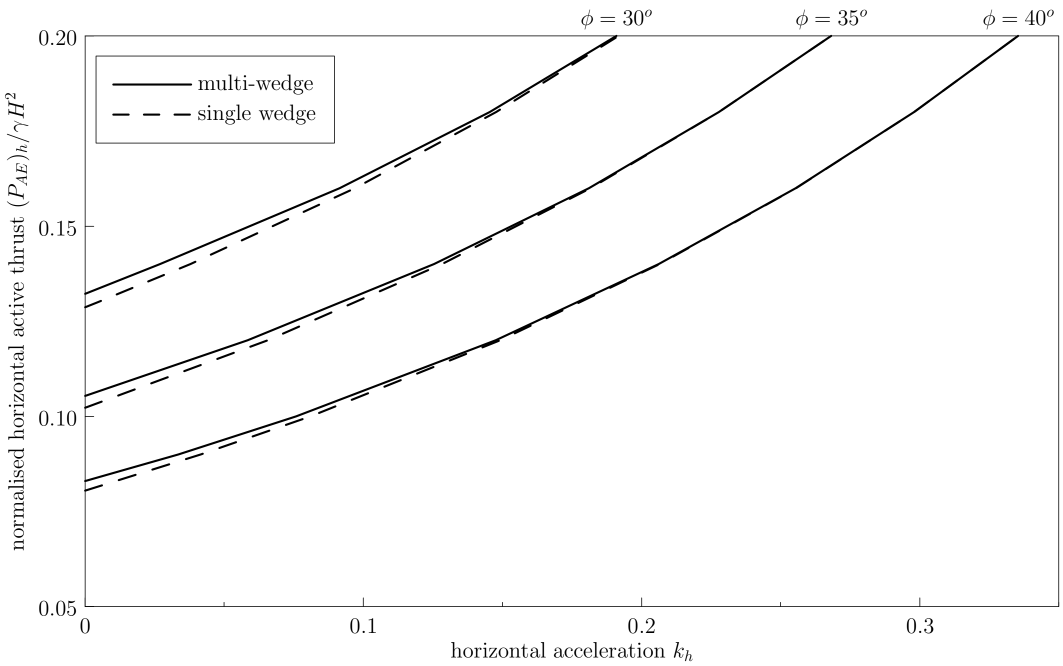

Figure 8: Plot of $P_{AE}\cos\delta'/\gamma H^2$ vs. k_h, for various ϕ' (30^o, 35^o, 40^o), $\delta' = \phi'$, $\beta = 0$. Both constrained (single wedge) and unconstrained (multiple wedge) analyses are plotted.

7. Combined sliding, bearing and overturning

The foregoing analyses assume that all deformation takes place along the horizontal base of the wall. However in reality failure modes may typically include soil beneath the wall. It is known that the static stability of a wall against combined sliding and bearing and combined sliding, bearing and overturning can be smaller than that against pure sliding and pure bearing considered separately. This is no different for the seismic case.

The flexibility of the DLO process is illustrated whereby the previous problem is repeated with soil modelled below the wall, for example as shown in Fig. 10. In this model, nodes were additionally placed within the solid below the wall (including its upper and right hand boundary) and on the lower boundary of the retained soil body. Sliding and bearing only models were modelled by constraining the DLO model to model translational mechanisms only. Sliding, bearing and overturning models were modelled by enabling rotations along edges (see Appendix A). In this example the

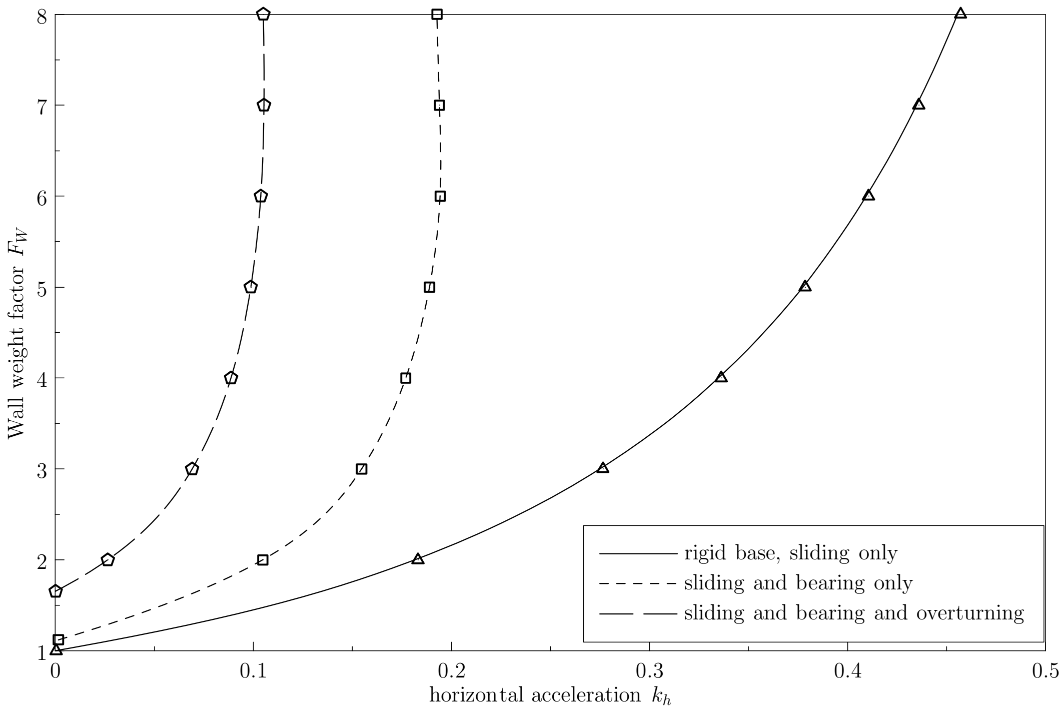

Figure 9: Plot of wall weight factor F_w (based on weight of wall required for static stability on a rigid base) against horizontal acceleration k_h for wall collapse including the effect of wall inertia. The solid line is derived from theory [5], and the dashed lines are interpolated between DLO data points (shown by symbols).

required horizontal acceleration for collapse reduces almost by a factor of 2 to 0.18g compared to that for pure sliding.

Results for a range of different wall weight ratios are given in Fig. 9, and clearly indicate the significant effect of combined sliding and bearing, and sliding, bearing and overturning on the threshold acceleration required for triggering instability or onset of permanent wall displacements.

It is noted that results for the latter cases would be significantly influenced by the wall width as well as its weight. In order to directly assess stability for bearing, sliding, and overturning, the required normalised wall weight $(W_w/\gamma H^2)$, where W_w is the weight of the wall, is plotted against horizontal acceleration for widths of wall equal to $0.5H$ and $1.0H$ in Fig. 11. It is seen that increased width of wall increases the acceleration at which instability occurs for a given wall weight and additionally suppresses overturning,

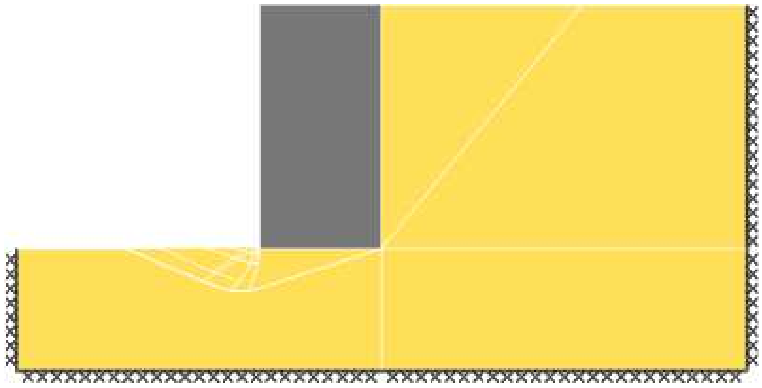

Figure 10: Sliding and bearing wedge failure mechanism for wall unit weight 1.052γ. This is 4 times the unit weight required for static collapse (in the pure sliding case only). The wall fails at $k_h = 0.177$. Soil below base, $\phi = \phi_b = 35^o, \delta = \phi/2,$. Mechanism avoids doing work against wall weight friction.

bringing the critical collapse mechanism closer to sliding and bearing failure.

8. Modelling of water pressures during seismic loading

8.1. Introduction

The presence of water is known to play an important role in determining the loads on retaining walls during earthquakes. Free water adjacent to a retaining wall can exert dynamic pressures on a wall and this pressure would need to be applied explicitly during a pseudo-static limit analysis calculation. Approaches such as those developed by *e.g.* Westergaard [18] may be adopted in this case.

When backfill is water saturated, accumulation of excess pore pressures due to dilatancy and dynamic fluctuation of pore water pressure due to inertia force should be taken into account. In a pseudo-static limit analysis, such water pressure distributions can be explicitly defined prior to the analysis and will affect the stability of the soil mass.

In addition, the transmission of inertial acceleration through saturated backfill must be considered. This will vary depending on the permeability of the backfill soil. Matsuzawa et al. [12] discussed these cases for high, intermediate and low permeability soils and gave guidance on the effective weight to be used in *e.g.* the Mononobe-Okabe equation. However for a

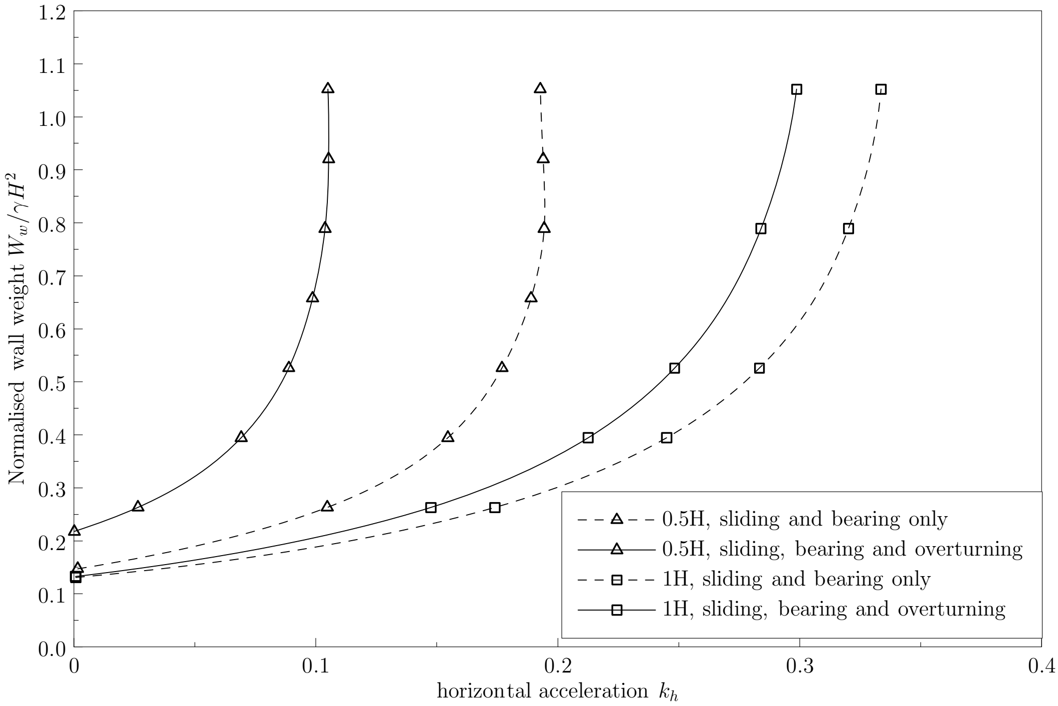

Figure 11: Plot of normalised wall weight against horizontal acceleration k_h for wall collapse including the effect of wall inertia. DLO models considered combined sliding and bearing failure, and combined sliding, bearing and toppling failure. Wall weight normalised by γH^2. Wall widths of $0.5H$ and $1.0H$ (where H = wall height) modelled ($\phi = \phi_b = 35^o, \delta = \phi/2$)

general purpose limit analysis, it is necessary to consider the seismic effects on the body forces and water pressures independently. This will be discussed in the following sections. The arguments presented are in terms of accelerations applied to a soil body from a base layer and thus strictly only apply to bodies of soil of infinite horizontal extent.

8.2. Effect of permeability of backfill soils

8.2.1. High permeability backfill soils

For this condition it is assumed that the pore water can move freely in the voids without any restriction from the soil particles (requiring also free draining boundaries). Thus the soil skeleton and the pore water are acted upon independently by the vertical and horizontal accelerations.

The vertical acceleration is assumed to be transmitted primarily by compression leading to a dynamic vertical force (including gravity) on a soil particle per unit volume of $\frac{G_s\gamma_w.1}{1+e}(1-k_v)$.

If the effect of the acceleration on the water is independent of the soil, and of any soil deformation, then it would also be expected that the pore water pressure would increase by $(1-k_v)$.

The dynamic vertical buoyancy force per unit volume acting on a soil particle would then be given by $\frac{\gamma_w.1}{1+e}(1-k_v)$ and the difference is thus $\frac{(G_s-1)\gamma_w}{1+e}(1-k_v) = (\gamma_{sat}-\gamma_w)(1-k_v)$.

Alternatively, in terms of body forces, the total vertical body force is given by:

$$F_V = \gamma_{sat}(1-k_v) \tag{10}$$

The effective unit weight of water becomes:

$$F_W = \gamma_w(1-k_v) \tag{11}$$

The effective vertical body force then becomes (assuming the effective stress principle remains valid):

$$F'_V = \gamma'(1-k_v) \tag{12}$$

The horizontal acceleration is assumed to act only on the solid portion of the soil element *i.e.* the accelerations are being transmitted predominantly by shear and the water experiences no induced horizontal acceleration from the soil particles. Thus the total horizontal body force becomes:

$$F_H = \frac{G_s\gamma_w}{1+e}k_h = \gamma_{dry}k_h \tag{13}$$

This is the same as the effective horizontal body force if the pore water pressure does not vary laterally.

The above derivations are in agreement with Matsuzawa et al. [12] who argue the case from a slightly different viewpoint.

8.2.2. Low permeability backfill soils

For this type of soil 'it is assumed that solid portion and the pore water portion of the soil element behave as a unit upon the application of seismic acceleration.' [12].

Specifically, the dynamic vertical force (including gravity) on both soil and water per unit volume will be given by $\frac{(G_s+e)\gamma_w}{1+e}(1-k_v)$.

Where immediate volume change of the soil is not possible due to restricted drainage, then the effective stress in the soil should be unchanged before and after application of the vertical acceleration (the total stresses and thus pore pressures may change).

Prior to acceleration the effective stress was governed by the buoyant unit weight. The vertical buoyancy force per unit volume acting on a soil particle is given by $\frac{(G_s-1)\gamma_w}{1+e}$. In the short term the effective stress and thus this quantity should not change. Hence upon acceleration, the 'buoyancy' force per unit volume is given by:

$$\frac{(G_s+e)\gamma_w}{1+e}(1-k_v) - \frac{(G_s-1)\gamma_w}{1+e} = \frac{(1+e)-k_v(G_s+e)\gamma_w}{1+e} = \gamma_w - k_v\gamma_{sat} \tag{14}$$

Alternatively, in terms of body forces, the total vertical body force F_V is given by equation 10 as before.

The effective unit weight of water becomes:

$$F_W = \gamma_w - k_v\gamma_{sat} \tag{15}$$

and the effective vertical body force is given by:

$$F_V' = \gamma' \tag{16}$$

The horizontal acceleration is assumed to act on the solid portion and the pore water portion of the soil element as a unit. Thus the horizontal body force becomes:

$$F_H = \gamma_{sat}k_h \tag{17}$$

This is in partial agreement with Matsuzawa et al. [12] who, however argue that 'the vertical component, F_V can be calculated by subtracting the dynamic buoyancy force acting on the whole soil from the total dynamic gravitational force of the whole soil, and thus it becomes $\gamma'(1-k_v)$' [12]. The implication is that the vertical acceleration acts only on the buoyant unit weight of the soil as for the high permeability case, while the horizontal acceleration acts on the whole soil. This again implies that the pore water pressure would change by a factor of $(1-k_v)$.

However it is argued that this cannot be so if the solid portion and the pore water portion of the soil element behave as a unit, there is no scope for pore pressures to establish equilibrium throughout the whole soil body.

8.2.3. Intermediate permeability backfill soils

The horizontal inertial body force, F_H can be described by the below equation, where m is defined by [12] as the volumetric ratio of restricted water (*i.e.* water carried along with the particles during seismic movement) to the whole of the void.

$$F_H = \frac{G_s + me}{1 + e} \gamma_w k_h \tag{18}$$

m may vary between 0 (representing high permeability soil) to 1 (representing low permeability soil). However implied interaction between the soil and water will also generate pore water pressures due to the horizontal accelerations.

For small m, the vertical body force and pore water pressures might remain as for high permeability soils. However examination of the equations for equivalent water body force for low and high permeability soils indicates that the pore water pressure might be considered to be given by the following:

$$F_W = \gamma_w (1 - k_v) - X k_v \gamma' \tag{19}$$

where X may vary between 0 (representing high permeability soil) to 1 (representing low permeability soil). It would be expected that $X = f(m)$ and as a first approximation, it could be assumed that $X = m$.

8.3. Proposed theoretical framework

In general, horizontal and vertical seismic accelerations will be transmitted differently through dry soil, saturated soil, solids and water. Correct modelling of these in a saturated soil system requires a fully coupled dynamic analysis of the soil water system. The aim of a limit analysis approach is to provide a simpler solution methodology. However, it should be flexible enough to allow a range of scenarios to be used subject to the choice of the engineer.

The following equations are proposed for use when modelling the effect of seismic accelerations on saturated soil systems. Effective accelerations to be applied to the bulk (saturated) unit weight of the soil are given as follows:

$$k_{h,eff} = M_{kh} k_h \tag{20}$$

$$k_{v,eff} = M_{kv} k_v \tag{21}$$

where the modification factors M_{kh} and M_{kv} are a function of the soil permeability.

For a general purpose limit analysis, water pressures must be fully defined spatially for all coordinates (x, z) in the problem domain. It is proposed that the following equation can be used to estimate appropriate water pressures, (though it could be questioned as to whether all the terms are strictly additive.)

$$u(x, z) = u_{static} + \Delta u_{kv} + \Delta u_{kh} + \Delta u_{ex} \tag{22}$$

where

$$u_{static} = \gamma_w z_w \tag{23}$$

and z_w is the depth below water table.

Δu_{kv} defines the additional pore water pressure induced by vertical accelerations:

$$\Delta u_{kv} = -w_{kv} k_v u_{static} \tag{24}$$

where w_{kv} is a modification factor that depends on the soil permeability. Thus equation 22 can also be written as:

$$u(x, z) = u_{static}(1 - w_{kv} k_v) + \Delta u_{kh} + \Delta u_{ex} \tag{25}$$

Δu_{kh} defines the additional pore water pressure induced by horizontal accelerations *e.g.* a modified form of Westergaard's solution (though it might be defined to also vary with x) :

$$\Delta u_{kh} = \frac{7}{8} k_h \gamma_w \sqrt{H z_w} \tag{26}$$

and Δu_{ex} arises from accumulation of excess pore pressures due to dilatancy and dynamic fluctuation of pore water pressure due to inertia forces, it may be represented by an excess pore pressure ratio r_u such that:

$$\Delta u_{ex} = r_u \sigma'_v \tag{27}$$

Suggested values to be used for the coefficients M_{kh}, M_{kv}, w_{kv} for the different scenarios discussed previously are given in Table 1.

	Matsuzawa et al. [12]			proposed equations		
	high	inter-mediate	low	high	inter-mediate	low
M_{kh}	$\gamma_{dry}/\gamma_{sat}$	$\frac{G_s+me}{G_s+e}$	1.0	$\gamma_{dry}/\gamma_{sat}$	$\frac{G_s+me}{G_s+e}$	1.0
M_{kv}	1.0	1.0	1.0	1.0	1.0	1.0
w_{kv}	1.0	1.0	1.0	1.0	$1+\frac{X\gamma'}{\gamma_w}$	γ_{sat}/γ_w*

Table 1: Choice of acceleration modification parameters for various permeability (drainage) conditions. (*for very low permeability soils, it would be anticipated that and undrained analysis is more appropriate and that water pressure is therefore not relevant).

The differences between Matsuzawa et al. and the proposed equations are perhaps not that significant in practice. For high permeability soils they are in agreement. For intermediate permeability soils it would be anticipated that the pore pressures would be dominated by the Δu_{ex} term in equation 22, and for low permeability soils, it would be expected that pore pressures would be dominated by those generated due to undrained shearing of the soil and that an undrained analysis was more relevant.

8.4. Example calculations and commentary

To highlight the differences in total earth pressures experienced by a wall, the scenarios in Table 1 were modelled using the simple wall model depicted in Fig. 2 and the results presented in Fig. 12 showing the significant influence of water pressure. For the scenarios involving water, it was assumed that the water table in the backfill coincided with the soil surface. Water pressures were not modelled beneath the wall. The theoretical calculations were based on the Mononobe-Okabe equations, using equivalent values of γ, k_h and k_v given in Appendix G. The effects of the additional water pressure terms Δu_{kh}, Δu_{ex} were not included.

It should be noted that when the water pressure is computed as $u = (1-k_v)\gamma_w z$ (as for example in all the Matsuzawa et al. cases) where z is the depth below the water table, the water force on the wall must be computed as:

$$P_W = \frac{1}{2}H^2\gamma_w(1-k_v) \tag{28}$$

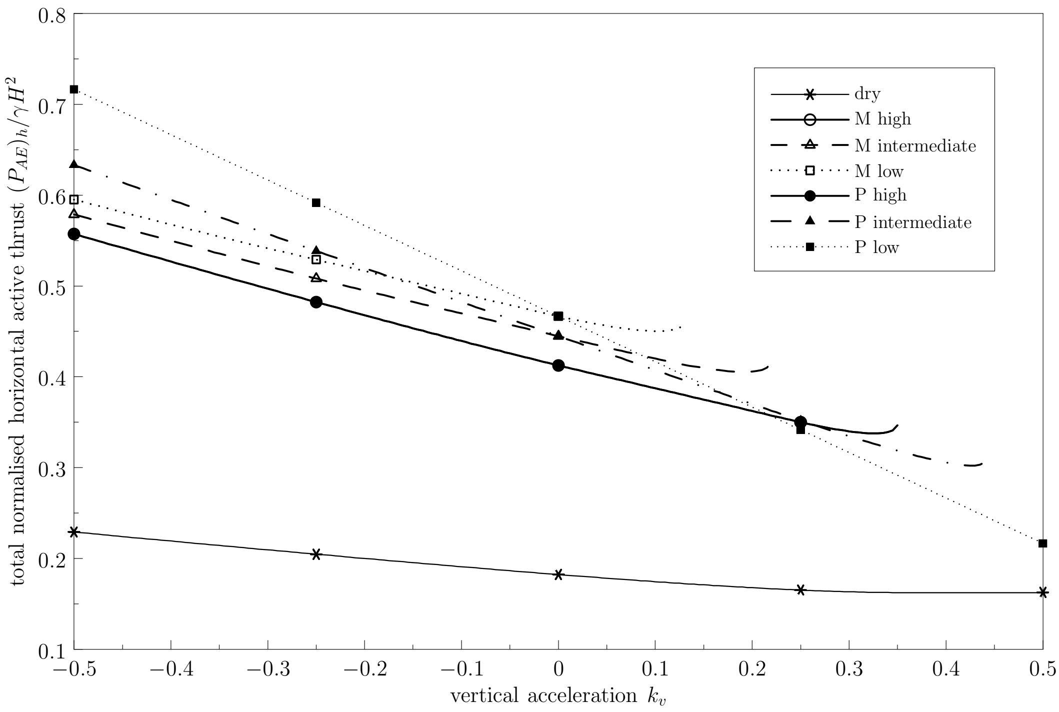

Figure 12: Plot of $(P_{AE})_h/\gamma_{sat}H^2$ vs. k_v, for different assumptions of water pressure at $k_h = 0.25$. P_{AE} is taken as the total horizontal earth pressure. $\gamma_{dry}/\gamma_{sat}$ taken as 0.75 and and γ'/γ_{sat} taken as 0.5. Δu_{kh} and Δu_{ex} taken as zero. For intermediate cases, $m = X = 0.5$. Theory (lines) and DLO results (symbols). Results given for Matsuzawa et al. analysis (M) and proposed analysis (P).

It is hard to find examples in the literature where this value is explicitly computed, otherwise previous literature remains ambiguous as to what to assume for the pore water pressures. It should however be noted that the dynamic behaviour of backfill soils is very complex involving biased initial stresses and relatively large lateral movements of the wall (and hence, volume expansion preventing the build-up of excess pore water pressures). Implementation of the proposed equations within a numerical limit analysis model and variation of the parameters M_{kh}, M_{kv}, w_{kv} allows the user flexibility to account for such possibilities if desired.

9. Case Study - Kobe Earthquake

In the 1995 Kobe earthquake, a large number of reclaimed islands in the port area of Kobe were shaken by a very strong earthquake motion. As indicated in Fig. 13, the recorded peak ground accelerations in the horizontal direction were of the order of 0.3-0.5 g, which reflects the proximity of the port to the causative fault in this magnitude 7.2 earthquake. The quay walls of the artificial islands are massive concrete caissons with a typical cross section shown in Fig. 14. During the earthquake, the quay walls moved about 2-4 m towards the sea ([19]; [20]). Both inertial loads due to ground shaking and liquefaction of the backfills and foundations soils (replaced sand in Fig. 14) contributed to the large seaward movement of the quay walls. Effects of liquefaction are beyond the scope of this paper, but rather two of the walls designed for very different levels of seismic loads will be comparatively examined using the limit analysis approach.

The location of the two walls is indicated in Fig. 13. The PI Wall (western part of Port Island) was designed with a seismic coefficient of 0.10, while the MW Wall (western part of Maya Wharf) was designated as a high seismic-resistant quay wall and was designed with a seismic coefficient of 0.25 ([19]). This design assumption resulted in a much larger width of the caisson of MW Wall (shown in Fig. 15) as compared to that of the PI Wall (shown in Fig. 14). Simplified models of the walls for limit analysis are shown in Fig. 16 and Fig. 17 respectively (including slip lines computed by DLO analysis), while model parameters required for the analysis are summarized in Table 2. Here, parameters for the backfills, replaced sand and foundation rubble were adopted from Iai et al. [21]), whereas clay properties were taken from Kazama et al. [22]. The key objective in the limit state analysis is to calculate the seismic coefficient k_h (or horizontal acceleration used for the equivalent static load) causing failure of the soil-wall system (collapse load), and assuming $k_v = 0$. Effects of wall inertia, discussed previously, were considered in the analyses. Results of the limit state analyses are presented in Fig. 18 with k_h plotted as a function of δ'/ϕ', where δ' is the interface friction between the wall base/vertical faces and the soil. For a δ'/ϕ' value of 0.66, the PI wall and Maya wall analyses predicted collapse horizontal accelerations of 0.12g and 0.23g respectively which is relatively close to those values intended by the designers (0.10g and 0.25g respectively). The analyses were undertaken assuming a value of $M_{kh} = 1.0$. If M_{kh} were taken as $\gamma_{dry}/\gamma_{sat}$, then the values of k_h for instability might be $\sim$10% higher for the PI wall and a few

% for the Maya wall (since its failure is dominated by the forward caisson).

The Maya wall appears to be more sensitive to changes in values of δ'/ϕ' than the PI wall. This is attributed to the nature of the failure mode. The Maya wall is dominated by sliding and so is significantly affected by changes in δ'. The PI wall fails primarily by forward rotation (sliding and overturning), and is thus only indirectly affected by δ' via the active earth pressure and the bearing capacity coefficient.

Soil type/caisson	ρ (t/m^3)	ϕ' (degrees)	c_u (kPa)	source
Backfill	1.8	36	-	[21]
Foundation soil (replaced)	1.8	37 (36)	-	[21]
Stone backfill	2.0	40	-	[21]
Foundation rubble	2.0	40	-	[21]
Clay (Port Island)	1.6-1.7	-	60 - 100	[22]
PI Equivalent Caisson	1.9	-	-	-
Maya Wharf Equivalent Caisson (new)	1.92	-	-	-
Maya Wharf Old cellular wall	2.0	-	-	-

Table 2: Model parameters used in PI and Maya wall analyses.

10. Conclusions

1. The theoretical extension of DLO to cover pseudo-static seismic loading has been described.
2. DLO has been verified against the Mononobe-Okabe solutions by constraining it to produce a single wedge solution. In certain extreme cases involving high horizontal accelerations, small differences can be observed that are dependent on implicit assumptions made about the problem kinematics.
3. When the DLO procedure is free to find the most critical mechanism, allowing more complex and realistic failure mechanisms to develop (*e.g.* multiple slip-planes, curved slip planes), it shows an increase in active pressure by up to 3% (for $\phi' = 40^o$) for the most critical case of a fully frictional wall/soil interface, horizontal soil surface, and zero horizontal acceleration.

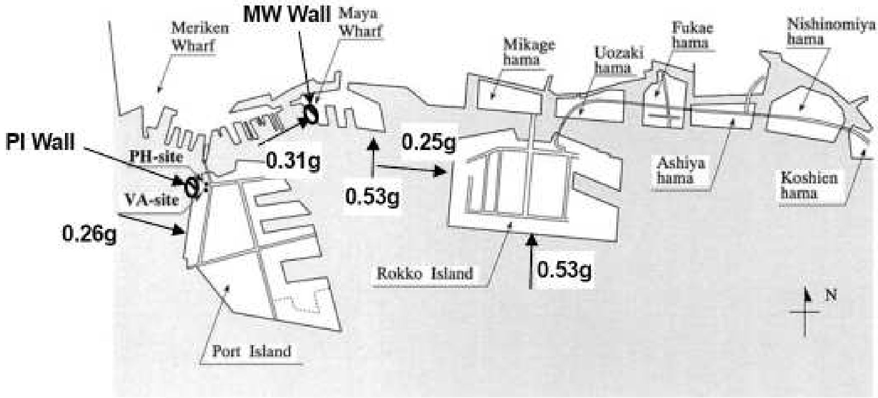

Figure 13: Estimates of horizontal peak ground accelerations on quay walls of reclaimed islands in the 1995 Kobe earthquake (acceleration values after Inagaki et al. [19])

4. Problems with wall inertia have been verified against the results of Richards and Elms. Wall inertia is shown to dramatically reduce the stability of retaining walls. Additional studies of combined sliding, bearing and overturning failure indicate that significant further reductions in stability can occur depending on the wall width.
5. The representation of water pressures in a numerical limit analysis has been examined. Comprehensive equations suitable for general purpose limit analysis have been proposed and two case studies from the literature have been examined.
6. The application of DLO to gravity retaining walls is expected to generate results that can be used in the context of approaches that adopt the methods of Mononobe-Okabe and Richard and Elms. The advantages of DLO lie in terms of its versatility to rigorously consider the geometry and collapse surfaces of complex engineering structures, such as those illustrated in the case studies in this paper.

A. Details of DLO analyses carried out in this paper

All analyses were carried out using the DLO based software LimitState:GEO [14]. All retaining walls were modelled as a 'Rigid' body. The soil was modelled as a Mohr-Coulomb material. Nodes (in addition to those at vertices) were selectively distributed in the problem as indicated in the text. with the

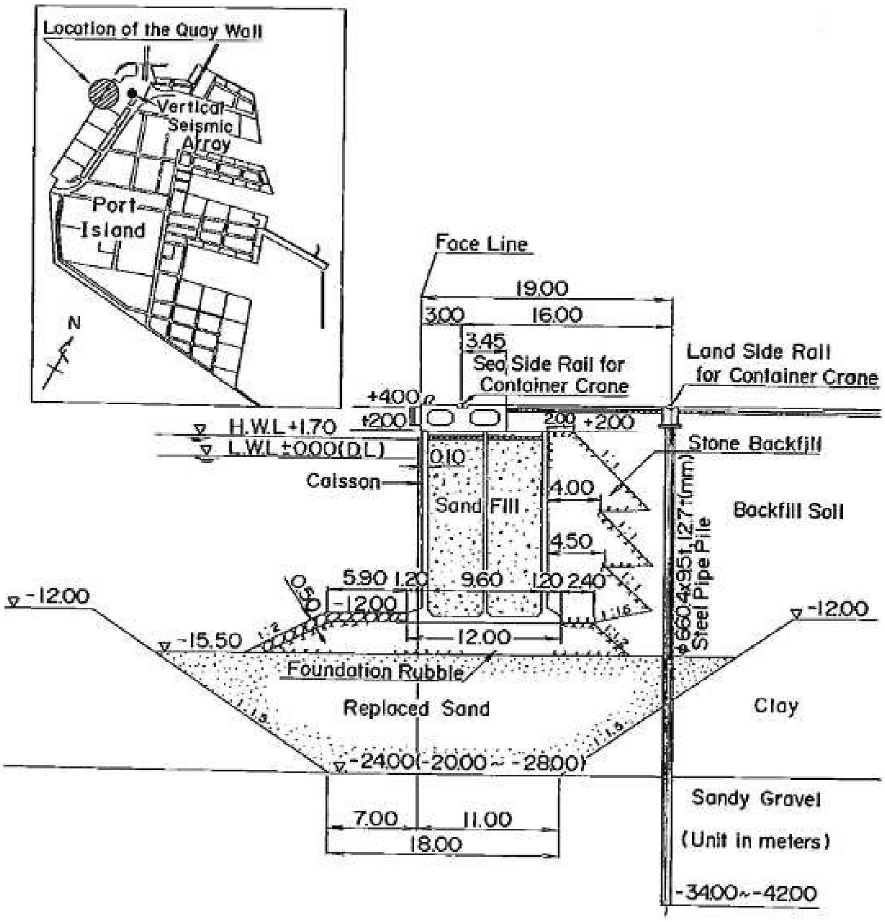

Figure 14: Cross section of a quay wall at Port Island (PI Wall) designed with a seismic coefficient of 0.10 [19]

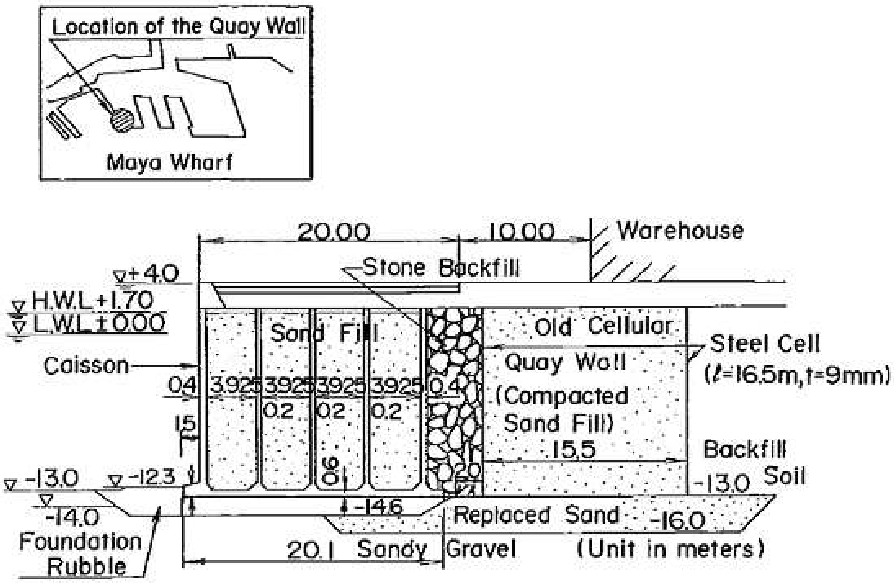

Figure 15: Cross section of a high seismic-resistant quay wall at Maya Wharf (MW Wall) designed with a seismic coefficient of 0.25 [19]

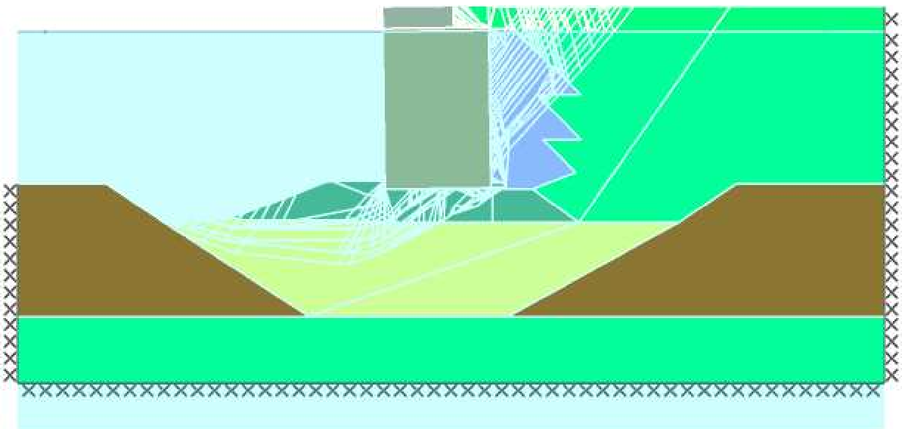

Figure 16: Example DLO analysis of the quay wall at Port Island (PI Wall) designed with a seismic coefficient of 0.10 [19]. Nodes were applied only to the solids (and adjacent boundaries) in which failure occurs. Some solids were split as illustrated to focus nodes to the areas where failure occurs.

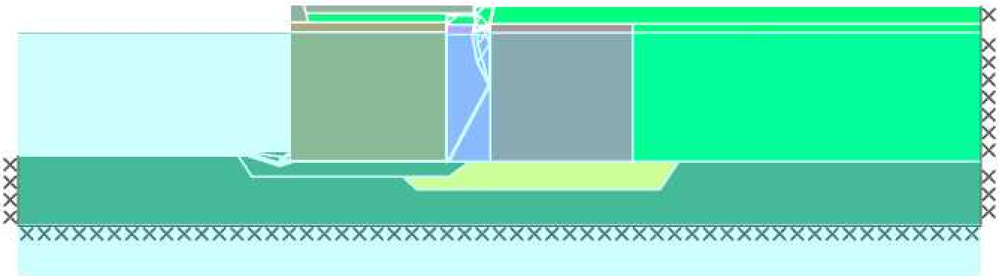

Figure 17: DLO analysis of the high seismic-resistant quay wall at Maya Wharf (MW Wall) designed with a seismic coefficient of 0.25 [19] .

nodal spacing on 'Boundaries' set at half that used in 'Solids'. All analyses utilized 1000 nodes with the exception of the sliding and bearing, and sliding, bearing and overturning analyses which utilized 2000 nodes. The sliding and bearing analyses were conducted using the 'Model Rotations' parameter set to 'False'. The sliding, bearing and overturning analyses were carried out with the 'Model Rotations' parameter set to 'Along edges'.

B. The Mononobe-Okabe pseudo-static model

The Mononobe-Okabe equation for the prediction of the total dynamic active thrust on a retaining wall is based on the equilibrium of a single Coulomb sliding wedge, as depicted in Fig. 19 where quasi-static vertical and horizontal inertial forces of the fill material are included.

The weight of the wedge (W) is given by:

$$W = \frac{1}{2}\gamma H^2 \frac{\cos(\theta-\beta)\cos(\theta-\alpha)}{\cos^2\theta\sin(\alpha-\beta)} \tag{29}$$

Force equilibrium gives the total active thrust (P_{AE}) :

$$P_{AE} = \frac{1}{2}K_{AE}\gamma H^2(1-k_v) \tag{30}$$

where the horizontal component is given by:

$$(P_{AE})_h = P_{AE}\cos(\delta' + \theta), \tag{31}$$

and

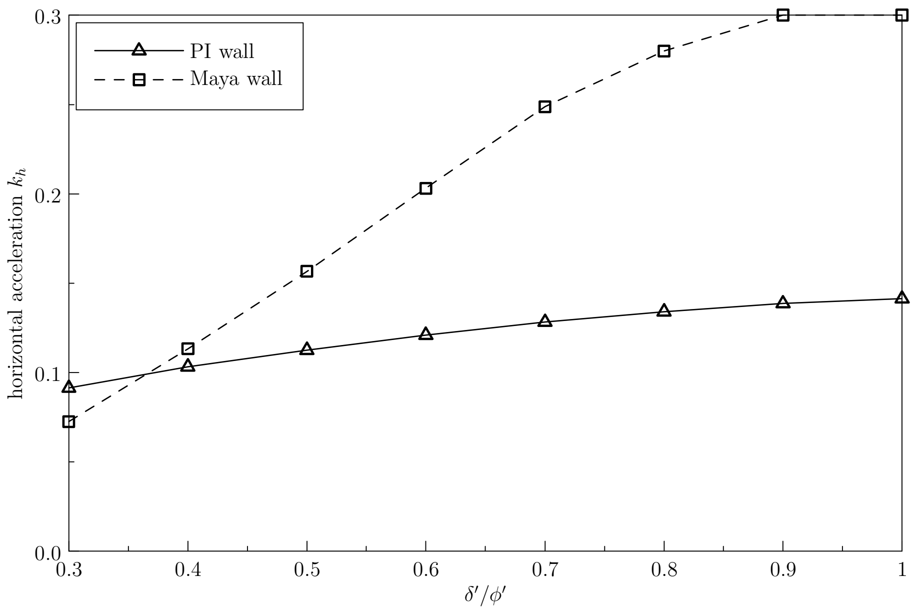

Figure 18: Variation of horizontal seismic acceleration required for instability with friction ratio on caisson base and walls

$$k_h = a_h/g \tag{32}$$

$$k_v = a_v/g \tag{33}$$

$$K_{AE} = \frac{\cos^2(\phi' - \theta - \psi)}{\cos\psi \cos^2\theta \cos(\delta' + \theta + \psi)\left[1 + \sqrt{\frac{\sin(\delta'+\phi)\sin(\phi'-\beta-\psi)}{\cos(\delta'+\theta+\psi)\cos(\beta-\theta)}}\right]^2} \tag{34}$$

$$\psi = \tan^{-1}[k_h/(1 - k_v)] \tag{35}$$

587 The angle α_{AE} of the wedge to the horizontal may be calculated as follows:

$$\alpha_{AE} = \phi' - \psi + \tan^{-1}\left[\frac{-\tan(\phi' - \psi - \beta) + C_{1E}}{C_{2E}}\right] \tag{36}$$

588 where:

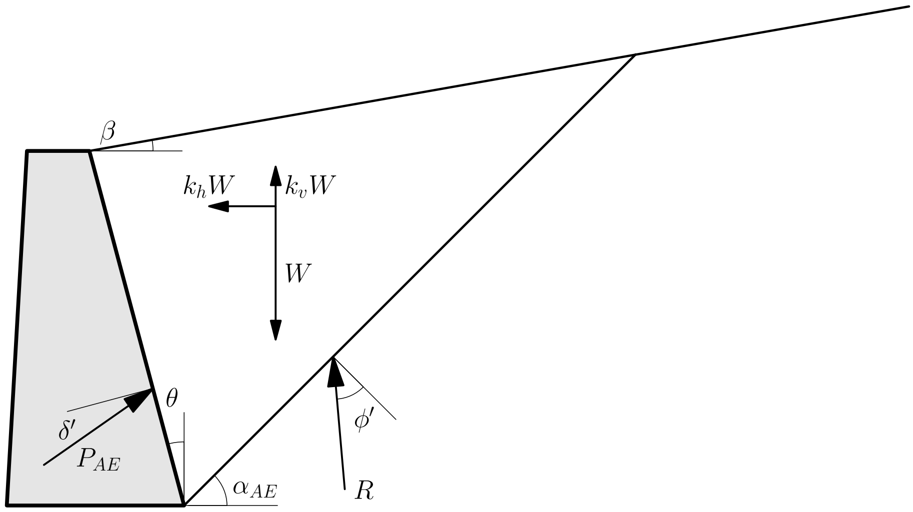

Figure 19: Coulomb wedge model used in Mononobe-Okabe solution

$$C_{1E} = \sqrt{\tan(\phi' - \psi - \beta)\left[\tan(\phi' - \psi - \beta) + \frac{1}{\tan(\phi' - \psi - \theta)}\right]\left[1 + \frac{\tan(\delta' + \psi + \theta)}{\tan(\phi' - \psi - \theta)}\right]} \tag{37}$$

589 and

$$C_{2E} = 1 + \left\{\tan(\delta' + \psi + \theta)\left[\tan(\phi' - \psi - \beta) + \frac{1}{\tan(\phi' - \psi - \theta)}\right]\right\} \tag{38}$$

C. Notation

a_v	vertical acceleration
a_h	horizontal acceleration
k_v	vertical seismic acceleration coefficient
k_h	horizontal seismic acceleration coefficient
w_{kv}	acceleration modification factors for pore pressure
F_w	Richard and Elms wall weight factor
H	wall height
K_{AE}	dynamic active earth pressure coefficient
M_{kh}	horizontal acceleration modification factor for soil weight
M_{kv}	vertical acceleration modification factor for soil weight
P_{AE}	active thrust
W_w	weight of the wall required for dynamic stability
α_{AE}	angle of critical failure surface
β	slope angle
γ	soil unit weight
ϕ'	effective angle of shearing resistance
ϕ'_b	effective angle of shearing resistance on base of wall
δ'	effective soil-wall interface angle of shearing resistance
ψ	$\tan^{-1}[k_h/(1-k_v)]$
θ	inclination of wall back to vertical

D. Limit equilibrium vs limit analysis

The Mononobe-Okabe equation is a limit equilibrium solution in that it does not explicitly consider the problem kinematics based on the normality condition, and therefore cannot be considered a true upper bound. In order to make comparisons with DLO (a limit analysis method) results it is therefore necessary to reanalyse the equation from a Limit Analysis standpoint.

Implicit in the Mononobe-Okabe analysis is the assumption that the vertical component of the wall/soil interaction force is directed downwards, thus implying that the soil moves downwards relative to the wall. In limit analysis this is only valid so long as $\alpha_{AE} > \phi'$ (see Fig. 19). Beyond this state, consideration of the kinematics, based on the associative flow rule required by limit analysis, yields the result that the soil wedge moves upwards as it slides. The Mononobe-Okabe model also makes no assumptions about the movement of the wall. If it is assumed that it moves horizontally only, then the direction of the active thrust tangential to the wall must start to reverse from the point at which $\alpha_{AE} = \phi'$.

Initially there is a transition stage, in which α_{AE} remains fixed and equal to ϕ'. In this case the wedge movement is purely horizontal and there is no relative movement between wedge and soil. ϕ' therefore does not have to be limiting and may vary as follows: $-\phi' < \delta' < \phi'$.

In this case the reaction force R on the wedge sliding face is orientated to the vertical and the horizontal component of the active thrust $(P_{AE})_h$ is independent of δ', and may be given by the following equation.

$$(P_{AE})_h = W k_h \tag{39}$$

Beyond the transition phase, the soil/wall friction fully reverses. This requires substitution of $(-\delta')$ for δ' in equations 30 and 36.

For pure horizontal wall movement, Mononobe-Okabe is therefore a limit analysis method up to the point of the transition phase, beyond which it is limit equilibrium, and the procedure to find maximum thrust is not strictly theoretically valid (though probably reasonable). For pure horizontal wall movement, the limit equilibrium approach is probably more realistic than the limit analysis approach, since soil dilation is usually a fraction of the angle of shearing resistance. However pure horizontal wall movement will only occur in limit analysis if the wall is resting on *e.g.* a cohesive clay. If it rests upon a cohesionless material, then the kinematics in a limit analysis will generally act to maintain the soil/wall friction downwards.

E. $c' - \phi'$ soil

The following equations are derived from those presented by Prakash [15] for the prediction of the total dynamic active thrust (P_{AE}) on a retaining wall retaining horizontal $c' - \phi'$ soil with a surface surcharge q. They have been modified to follow the notation in this paper and to separately account for soil cohesion intercept c' and soil-wall interface cohesion intercept c'_w.

$$P_{AE} = \gamma H_s^2 N_{a\gamma} + q H_s N_{aq} - c' H_s N_{ac} \tag{40}$$

where

$$N_{a\gamma} = \frac{[(n+\frac{1}{2})(\tan\theta + \cot\alpha_{AE}) + n^2\tan\theta][\sin(\alpha_{AE}-\phi') + k_h\cos(\alpha_{AE}-\phi')]}{\cos(\alpha_{AE}-\phi'-\theta-\delta)} \tag{41}$$

$$N_{aq} = \frac{[(n+1)\tan\theta + \cot\alpha_{AE})][\sin(\alpha_{AE}-\phi') + k_h\cos(\alpha-\phi')]}{\cos(\alpha_{AE}-\phi'-\theta-\delta)} \tag{42}$$

$$N_{ac} = \frac{\cos\phi'\csc\alpha_{AE} + \frac{c'_w}{c'}\sin(\alpha_{AE}-\phi'-\theta)\sec\theta}{\cos(\alpha_{AE}-\phi'-\theta-\delta)} \tag{43}$$

The parameter n allows for the inclusion of a tension crack in the analysis such that if the depth of the tension crack is H_c, then

$$H_c = n(H - H_s) \tag{44}$$

where H is the height of the retaining wall and H_s is the depth of soil from the base of the tension crack to the base of the wall.

It is necessary to find the angle α_{AE} that gives the minimum value of P_{AE}. Prakash [15] presents separately optimized coefficients $N_{a\gamma}$, N_{aq}, and N_{ac}, however it is not possible to compare these results directly with a DLO analysis since all three coefficients should be considered together in the optimization. Instead in this paper all three components were numerically optimized simultaneously.

F. The Richard and Elms pseudo-static model

Richard and Elms [5] extended the Mononobe-Okabe model to include the effect of wall inertia. They introduced a safety factor F_w on the weight of the wall such that

$$F_w = F_T F_I = \frac{W_w}{W_{w0}} \tag{45}$$

where W_{w0} is the weight of the wall required for equilibrium in the static case and W_w is the weight of the wall required for equilibrium under seismic acceleration. F_T is a soil thrust factor defined as follows:

$$F_T = \frac{K_{AE}(1-k_v)}{K_A} \tag{46}$$

where $K_A = K_{AE}$ when $\psi = 0$.

F_I is a wall inertia factor defined as follows:

$$F_I = \frac{C_{IE}}{C_I} \tag{47}$$

where

$$C_{IE} = \frac{\cos(\delta' + \theta) - \sin(\delta' + \theta)\tan\phi'_b}{(1 - k_v)(\tan\phi'_b - \tan\psi)} \tag{48}$$

and $C_I = C_{IE}$ when $k_h = k_v = 0$. $\tan\phi'_b$ is the angle of shearing resistance on the base of the wall. It assumed that it slides on a rigid base.

G. Equivalent Mononobe-Okabe parameters for water model

To use the general water model in a conventional Mononobe-Okabe equation, it is necessary to adopt the following equivalent parameters, where the subscript $_{MO}$ is used to denote the equivalent Mononobe-Okabe parameter:

Consideration of the case where $k_h = k_v = 0$ gives:

$$\gamma_{MO} = \gamma' \tag{49}$$

Since M_{kh} is defined in terms of γ_{sat} then:

$$k_{h_{MO}} = k_h M_{kh} \gamma_{sat}/\gamma' \tag{50}$$

During seismic accelerations, the effective weight of the soil is given by:

$$\gamma'_{seismic} = \gamma_{sat}(1 - M_{kv}k_v) - \gamma_w(1 - w_{kv}k_v) \tag{51}$$

$$\gamma'_{seismic} = \gamma'\left(1 - k_v\frac{\gamma_{sat}M_{kv} - \gamma_w w_{kv}}{\gamma'}\right) \tag{52}$$

Hence

$$k_{v_{MO}} = k_v\frac{\gamma_{sat}M_{kv} - \gamma_w w_{kv}}{\gamma'} \tag{53}$$

References

[1] S. Iai, Recent studies on seismic analysis and design of retaining structures, in: Proc. 4th Int. Conf. on Recent Advances in Geotechnical Earthquake Engineering and Soil Dynamics, San Diego, Paper No. SOAP4, 2001, pp. 1–28.

[2] N. Mononobe, H. Matsuo, On the determinations of the earth pressure during earthquakes, in: Proc. World Engineering Conference, Tokyo, Vol. 9, 1929, pp. 176–185.

[3] S. Okabe, General theory of earth pressure on earth pressure and seismic stability of retaining wall and dam, Journal of the Japanese Society of Civil Engineers 10 (6) (1924) 1277–1323.

[4] N. Newmark, Effects of earthquakes on dams and embankments, 5th Rankine Lecture, Geotechnique 15 (2) (1965) 139–160.

[5] R. Richards, D. Elms, Seismic behaviour of gravity retaining walls, ASCE Journal of the Geotechnical Engineering Division 105 (GT4) (1979) 449–464.

[6] M. Ichihara, H. Matsuzawa, Earth pressure during earthquake, Soils and Foundations 13 (4) (1973) 75–86.

[7] I. Ishibashi, Y.-S. Fang, Dynamic earth pressures with different wall movement modes, Soils and Foundations 27 (4) (1987) 11–22.

[8] J. Koseki, F. Tatsuoka, Y. Munaf, M. Tateyama, K. K., A modified procedure to evaluate active earth pressure at high seismic loads, Soils and Foundations, Special Issue No. 2 on Geotechnical Aspects of the Hyogoken-Nambu Earthquake (1998) 209–216.

[9] H. Hazarika, Prediction of seismic active earth pressure using curved failure surface with localized strain, American J. of Engineering and Applied Science 2 (3) (2009) 544–558.

[10] M. Cubrinovski, B. Bradley, Evaluation of seismic performance of geotechnical structures, in: Theme Lecture, Int. Conf. on Performance-Based Design in Earthquake Geotechnical Engineering, IS-Tokyo2009, 15-17 June, Tsukuba, Japan, 2009, pp. 121–136.

[11] S. Kramer, Performance based earthquake engineering: Opportunities and implications for geotechnical engineering practice, in: Proc. Geotechnical Earthquake Engineering and Soil Dynamics IV: Keynote. Sacramento, CA (USA). Geotechnical Special Publication GSP 181, 2008, pp. 1–32.

[12] H. Matsuzawa, I. Ishibashi, M. Kawamura, Dynamic soil and water pressures of submerged soils, ASCE Journal of Geotechnical Engineering 111 (10) (1985) 1161–1176.

[13] C. C. Smith, M. Gilbert, Application of discontinuity layout optimization to plane plasticity problems, Proceedings of the Royal Society A: Mathematical, Physical and Engineering Sciences 463 (2086) (2007) 2461–2484.

[14] LimitState Ltd, LimitState:GEO Manual VERSION 2.0, September 2009 Edition (2009).

[15] S. Prakash, Soil Dynamics, McGraw Hill, New York., 1981.

[16] H. Hazarika, H. Matsuzawa, Coupled shear band method and its application to the seismic earth pressure problems, Soils and Foundations 37 (3) (1997) 65–77.

[17] S. Nakamura, Re-examination of Mononobe-Okabe theory of gravity retaining walls using centrifuge model tests, Soils and Foundations 46 (2) (2006) 135–146.

[18] H. Westergaard, Water pressures on dams during earthquakes, Transactions ASCE 59 (8, Part 3) (1933) 418–472.

[19] H. Inagaki, S. Iai, T. Sugano, H. Yamazaki, T. Inatomi, Performance of caisson type quay walls at Kobe Port, Soils and Foundations, Special Issue on Geotechnical Aspects of the January 17 1995 Hyogoken-Nambu Earthquake (1996) 119–136.

[20] K. Ishihara, M. Cubrinovski, Performance of quay wall structures during the 1995 Kobe earthquake, Keynote paper 1, in: Proc. Int. Conf. on Offshore and Nearshore Geotechnical Engineering, GEOshore, Mumbai, India, 1999, pp. 23–24.

[21] S. Iai, K. Ichii, H. Liu, T. Morita, Effective stress analyses of port structures, Soils and Foundations, Special Issue on Geotechnical Aspects of the January 17 1995 Hyogo-Ken Nambu Earthquake (2) (1998) 97–114.

[22] M. Kazama, A. Yamaguchi, E. Yanagisawa, Seismic behaviour of underlying clay on man-made islands during the 1995 Hyogoken-Nambu Earthquake, Soils and Foundations, Special Issue on Geotechnical Aspects of the January 17 1995 Hyogo-Ken Nambu Earthquake 2 (1998) 23–32.